Flavin Reductase P: Structure of a Dimeric Enzyme That Reduces Flavin[†,‡]

John J. Tanner, Benfang Lei, Shiao-Chun Tu, and Kurt L. Krause*

Department of Biochemical and Biophysical Sciences, University of Houston, Houston, Texas 77204-5934

Received June 12, 1996; Revised Manuscript Received August 8, 1996[⊗]

ABSTRACT: We report the structure of an NADPH:FMN oxidoreductase (flavin reductase P) that is involved in bioluminescence by providing reduced FMN to luciferase. The 1.8 Å crystal structure of flavin reductase P from *Vibrio harveyi* was solved by multiple isomorphous replacement and reveals that the enzyme is a unique dimer of interlocking subunits, with 9352 Å^2 of surface area buried in the dimer interface. Each subunit comprises two domains. The first domain consists of a four-stranded antiparallel β-sheet flanked by helices on either side. The second domain reaches out from one subunit and embraces the other subunit and is responsible for interlocking the two subunits. Our structure explains why flavin reductase P is specific for FMN as cofactor. FMN is recognized and tightly bound by a network of 16 hydrogen bonds, while steric considerations prevent the binding of FAD. A flexible loop containing a Lys and an Arg could account for the NADPH specificity. The structure reveals information about several aspects of the catalytic mechanism. For example, we show that the first step in catalysis, which is hydride transfer from C4 of NADPH to cofactor FMN, involves addition to the *re* face of the FMN, probably at the N5 position. The limited accessibility of the FMN binding pocket and the extensive FMN−protein hydrogen bond network are consistent with the observed ping-pong bisubstrate−biproduct reaction kinetics. Finally, we propose a model for how flavin reductase P might shuttle electrons between NADPH and luciferase.

NAD(P)H:flavin oxidoreductases (flavin reductases) catalyze the reduction of flavin by NAD(P)H. The reduced flavin product is essential to a variety of biological functions such as bacterial bioluminescence (Tu & Mager, 1995), iron release from ferrisiderophores (Hallé & Meyer, 1992; Covès & Fontecave, 1993), activation of ribonucleotide reductase (Fontecave et al., 1987; Covès et al., 1993) and chorismate synthase (Hasan & Nestor, 1978), reduction of methemoglobin (Quandt et al., 1991; Chikuba et al., 1994), and oxygen activation (Gaudu et al., 1994).

It has been proposed that flavin reductases be identified as FRP for those specific for NADPH, FRD for those with a preference for NADH, and FRG for those that use both NADH and NADPH with similar efficiencies (Lei et al., 1994). Flavin reductases can also be divided into two subclasses on the basis of prosthetic group content. For example, FRE from *Escherichia coli* (Fontecave et al., 1987) has no detectable prosthetic group, whereas *Vibrio harveyi* FRP (Lei et al., 1994) and *Photobacterium* (formerly *Vibrio*) *fischeri* FRG (Inouye, 1994) have a noncovalently bound flavin cofactor.

Much of the interest in flavin reductases concerns elucidation of their role in bacterial bioluminescence. Flavin reductases D, P, and G have been detected in luminous bacteria, and some are believed to provide reduced FMN ($FMNH_2$) to luciferase in vivo as a substrate for the luminescence reaction (eqs 1 and 2).

$$\mathrm{FMN + NAD(P)H + H^+ \xrightarrow{\text{flavin reductase}} FMNH_2 + NAD(P)^+} \quad (1)$$

$$\mathrm{FMNH_2 + RCHO + O_2 \xrightarrow{\text{bacterial luciferase}} FMN + RCOOH + H_2O + light} \quad (2)$$

Flavin reductases in luminous bacteria differ in their affinities for FMN substrate, kinetic mechanisms, and putative interactions with luciferase. FRG has been isolated from *P. fischeri* as the major flavin reductase species (Inouye, 1994) and from *V. harveyi* as a minor species (Watanabe & Hastings, 1982). The former enzyme has a bound FMN cofactor (Inouye, 1994) and exhibits a ping-pong kinetic pattern (Tu et al., 1979), whereas the latter reductase lacks a prosthetic group and follows a sequential mechanism (Watanabe & Hastings, 1982). FRD has been detected in several species of luminous bacteria (Zenno & Saigo, 1994), but these enzymes do not bind a flavin cofactor. In this flavin reductase group, the kinetic mechanism has only been elucidated for the *V. harveyi* FRD, and it is of the sequential bisubstrate−biproduct type (Gerlo & Charlier, 1975; Michaliszyn et al., 1977; Jablonski & DeLuca, 1978; Watanabe & Hastings, 1982).

FRP, which is the subject of this work, is unique in several aspects. First, FRP has only been detected in *V. harveyi*. Second, the *V. harveyi* FRP was the first flavin reductase shown to have a bound flavin cofactor (Lei et al., 1994). Third, FRP displays an intriguing shift in kinetic mechanism when coupled in vitro to the luciferase light generation reaction. In the absence of luciferase FRP displays kinetic profiles consistent with a ping-pong bisubstrate−biproduct

[†] This work was supported by the National Institutes of Health (GM25953, S.-C.T.), the Robert A. Welch Foundation (E-1030, S.-C.T.), the State of Texas (K.L.K. and S.-C.T.), and the W. M. Keck Foundation.

[‡] Coordinates have been deposited in the Brookhaven Protein Data Bank and assigned the ID code 1CUM.

* Corresponding author. Email: kkrause@uh.edu.

[⊗] Abstract published in *Advance ACS Abstracts,* October 1, 1996.

[1] Abbreviations: FRP, flavin reductase P; FRD, flavin reductase D; FRG, flavin reductase G; NOX, NADH oxidase; MIR, multiple isomorphous replacement; RMSD, root mean square differences; NCS, noncrystallographic symmetry; A_s, solvent-accessible surface area.

S0006-2960(96)01400-6 CCC: $12.00

reaction mechanism. However, if the reaction is followed in the presence of luciferase by measuring light emission, the kinetic profile is consistent with a sequential reaction mechanism. This apparent shift in mechanism has been used as evidence that the reduced FMN cofactor of FRP is transferred to luciferase via a FRP−luciferase complex (Lei & Tu, 1994). The structural nature of this putative protein−protein complex, however, is unknown.

We report the 1.8 Å crystal structure of FRP from *V. harveyi* determined using multiple isomorphous replacement (MIR). FRP uses NADPH exclusively ($K_m = 20\ \mu M$), binds one FMN cofactor per monomer ($K_d = 0.17\ \mu M$), and has monomer molecular weight of 26 312. This is the first structure of a flavin reductase, and it belongs to a new structural class of flavoenzyme that also includes NADH oxidase (NOX) from *Thermus thermophilus* (Hecht et al., 1995).

The crystal structure of FRP is a dimer of interlocking subunits, with the FMN cofactor bound in the dimer interface. We use the structure to explain several aspects of catalysis, including FMN cofactor and NADPH substrate specificities, geometry of hydride transfer from NADPH to FMN, and the shift in kinetic mechanism in the luciferase-coupled assay.

MATERIALS AND METHODS

Crystallization and X-ray Data Collection. Purification, crystallization, and space group determination of FRP from *V. harveyi* cloned in *E. coli* were described elsewhere (Tanner et al., 1994). The enzyme was crystallized at room temperature in sitting drops equilibrated over a reservoir solution containing 30% poly(ethylene glycol) 6000 and 0.1 M Hepes, pH 7.0. The space group is $P2_1$ with cell dimensions $a = 51.2$ Å, $b = 85.9$ Å, $c = 58.1$ Å, and $\beta = 109.3°$. The asymmetric unit contains one homodimer.

One native and several heavy atom derivative data sets for MIR phase determination were collected to 2.6 Å resolution at 14 °C using a FAST area detector coupled to a Rigaku rotating anode operating at 50 kV and 180 mA with a 0.5 mm collimator. The detector distance was 80 mm and the 2θ angle was $-17°$. The data were collected by scanning about an axis 30° from a^* with a frame width of 0.1°. All FAST data sets were processed with MADNES (Messerschmidt & Pflugrath, 1987) and XSCALE (Kabsch, 1988).

Collection of the trimethyllead acetate derivative on the FAST was optimized for accurate measurement of anomalous scattering differences using the inverse beam method as follows. First, a 30° wedge of data was collected starting at the goniometer position (ω_1, χ, ϕ). Second, the Friedel mates of these data were collected in a 30° wedge starting at (ω_1, $-\chi$, $\phi + 180°$). The goniometer was then advanced to ($\omega_2 = \omega_1 + 25°$, χ, ϕ) and another pair of 30° slices were collected starting from goniometer positions (ω_2, χ, ϕ) and (ω_2, $-\chi$, $\phi + 180°$). The procedure was repeated for a total of 12 wedges or 360° of data. As with the Pt and native data sets, all data were collected about an axis 30° from a^* with a 0.1° frame width. Anomalous differences were calculated only from Friedel pairs obtained in temporally adjacent scans to minimize errors due to absorption and crystal decay.

A 1.8 Å native data set for structure refinement was collected at 4 °C using an R-axis II imaging plate coupled to a Siemens rotating anode operated at 50 kV and 90 mA with a 0.3 mm collimator. The detector distance was 90 mm and the 2θ angle was 0°. A total of 110 frames was collected with a 1.5° frame width. Standard Rigaku R-axis software was used to collect and process the data (Higashi, 1990; Tanner & Krause, 1994). See Table 1 for data collection statistics.

Table 1: Diffraction Data and MIR Analysis

	native		$(CH_3)_3PbOOCCH_3$, FAST	K_2PtCl_4, FAST
	R-axis	FAST		
concn (mM)			10.0	0.75
soaking time (days)			12	0.7
no. of observations	117092	27508	39833	19252
unique reflections	36163	13441	13013	13117
R-sym (%)[a]	4.3	2.3	3.5	2.0
completeness				
2.6 Å (%)	95.3	88.4	85.6	86.4
2.0 Å (%)	91.6			
1.8 Å (%)	81.9			
outer 0.1 Å shell (%)	40.7	51.8	47.0	50.4
R-merge (%)[b]			12.6	9.0
no. of sites			2	7
phasing power to 2.6 Å[c]			2.5 (2.7)[d]	1.7

[a] $R\text{-sym} = \sum\sum(|I(h)_i - \langle I(h)\rangle|)/\sum\sum I(h)_i$, where $I(h)_i$ is the intensity of the ith observation of reflection h and $\langle I(h)\rangle$ is the mean intensity of all equivalent measurements of reflection h. The summation is over all reflections. [b] $R\text{-merge} = \sum(|F(h)_d - F(h)_n|)/\sum F(h)_n$, where $F(h)_d$ and $F(h)_n$ are the scaled observed structure factor amplitudes for the derivative and native reflection h. The sum is over all reflections. [c] Phasing power $= \langle|FH|\rangle/\langle E\rangle$ for isomorphous data and $\langle 2|FH''|\rangle/\langle E\rangle$ for anomalous data, where $|FH|$ is the calculated heavy atom structure factor amplitude, $|FH''|$ is the contribution to $|FH|$ arising from the imaginary component of the heavy atom scattering factors, and E is the residual lack of closure. [d] Phasing power calculated from anomalous data is given in parentheses.

Phase Determination. Heavy atom soaks were carried out in the reservoir solution. Calculation of phases, heavy atom refinement, solvent flattening, and noncrystallographic symmetry (NCS) averaging were done with the PHASES program package (Furey & Swaminathan, 1995). Additional density modification was performed with SQUASH (Zhang & Main, 1990).

The structure was solved using isomorphous and anomalous data from a trimethyllead acetate derivative and isomorphous data from a K_2PtCl_4 derivative. The heavy atom positions of the two-site Pb derivative were found by inspection of an isomorphous difference Patterson map. The anomalous difference Patterson map gave identical results for the Pb positions. The seven sites of the K_2PtCl_4 derivative were found from difference Fourier maps.

Refinement of heavy atom parameters resulted in a phase set with a mean figure of merit of 0.71 to 2.6 Å resolution. A few helices and strands could be seen in the corresponding electron density map, but the entire chain could not be traced, nor could the amino acid sequence be identified. Phases were improved with density modification, including NCS averaging about the 2-fold axis of the dimer.

The 2-fold NCS transformation was determined as follows. The orientation of the 2-fold axis was found from a self-rotation function calculated in X-PLOR version 3.1 (Brünger, 1992), which showed a clear 5σ peak at spherical polar angles $\psi = 101°$, $\phi = 34°$, $\kappa = 182°$. The location of the NCS 2-fold axis was assumed to be the centroid of the dimer, which was estimated to be $x = 8$ Å, $y = 8$ Å, $z = 69$ Å (orthogonal coordinates) from inspection of an electron

density map covering the entire unit cell. After refinement of the NCS relation in PHASES, the electron density correlation coefficient was 0.74.

Solvent flattening, NCS averaging, and phase extension to 2.6 Å resulted in phases with a mean figure of merit of 0.83. Another round of density modification was performed with SQUASH using the 1.8 Å R-axis native data set. The quality of the electron density was markedly improved and several α-helices, β-strands, and connecting loops could be seen. Density for the FMN cofactor was unmistakable, and most of the amino acid sequence could be identified.

A C_α trace was built in O (Jones et al., 1991) using skeletonized representations of the 2.6 Å NCS averaged map and the 1.8 Å SQUASH-modified map. Next, a polyalanine model was constructed for the entire protein except for residues 1−3 (both subunits), 19−21 (B subunit), and 197−211 (both subunits). Two FMN molecules and side chains for all but 73 of the modeled residues were included in this initial MIR model.

Structure Refinement. The initial model was refined with simulated annealing and conjugate gradient positional refinement using X-PLOR and the Engh and Huber force field (Engh & Huber, 1991). The force field was modified by eliminating all hydrogen atoms, disabling the nonbonded electrostatic energy term, and using the repel nonbonded function with the parameters repel = 1.0, rexp = 4.0, irex = 1.0, and rcon = 16.0. This protocol was designed to minimize force field bias in subsequent calculations of hydrogen bonds and salt links. Individual *B*-factors were refined using restraints to standard deviations of 1.0 Å^2 for main chain bonded atoms, 1.5 Å^2 for side chain bonded atoms, 1.5 Å^2 for main chain atoms related by bond angles, and 2.0 Å^2 for side chain atoms related by bond angles. NCS restraints were not used during refinement. O and FRODO (Jones, 1978) were used for model building.

Water was added during the final stages of refinement. Solvent sites were filled if they had at least a 3σ peak in the $F_o - F_c$ map and at least a 1σ peak in the $2F_o - F_c$ map. Water was inspected after refinement, and those with either $B > 35$ Å^2 or that had weak or nonspherical $2F_o - F_c$ density were discarded.

A PO_4 anion (1 per subunit) was built into electron density near the *re* face of the FMN. The density was tetrahedral in shape and was present in the 1.8 Å MIR/density-modified map at 5σ. After the protein and 72 water molecules had been built, density for the unbuilt phosphates appeared at 4σ in the $2F_o - F_c$ map and 9σ in the $F_o - F_c$ map. Initially, we modeled a water molecule at the site, but positive $F_o - F_c$ density, which retained the tetrahedral shape, returned after refinement. The likely source of the phosphate ion that we observe is the phosphate buffer that was used in the final step of protein purification. Addition of the two PO_4 molecules decreased R_{free} by 0.2%.

The current model consists of 3564 atoms, including 460 amino acid residues, 2 FMN molecules, 2 PO_4 ions, and 107 water molecules. Residue 1 and residues 201−209 of both subunits were omitted from the model because of weak density. Also, 40 surface side chains were omitted due to weak density.

The conventional *R*-factor is 17.5% for 32 144 reflections between 28 and 1.8 Å resolution using a bulk solvent mask calculated using X-PLOR. The *R*-factor for 3540 randomly chosen reflections that had never been used in refinement

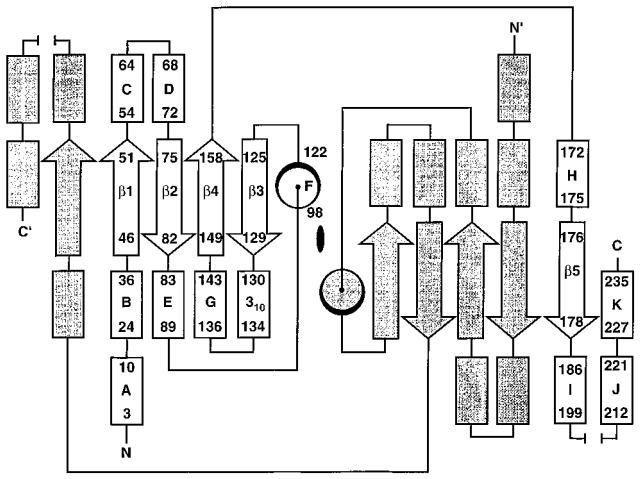

FIGURE 1: Topology diagram of the dimer. Arrows denote β-strands and rectangles α-helices. The circles in the middle of the diagram denote the F helices. The 2-fold axis is shown as a black oval.

(R_{free}) is 20.7%. The average real space correlation coefficient (Jones et al., 1991) between the model (all atoms) and the final $2F_o - F_c$ map is 0.95, and the standard deviation is 0.026. A Luzzati plot suggests a mean positional error of about 0.20 Å (Luzzati, 1952). The root mean square deviation from the ideal force field values is 0.013 Å for bonds, 1.5° for angles, and 22.8° for dihedral angles. The stereochemistry meets or exceeds all main chain and side chain tests of PROCHECK (Laskowski et al., 1993). All but 3 of the 404 non-glycine residues fall into the most favored or additional allowed regions of the Ramachandaran plot. The 3 outliers are in loops.

Analysis. Analyses of solvent-accessible surface area (A_s), salt links, hydrogen bonds, and root mean square differences (RMSD) were done with X-PLOR. The probe radius for A_s calculations was 1.4 Å, and the X-PLOR numerical accuracy parameter was set to 0.025. Water, PO_4, and FMN were excluded from calculations of the A_s buried in the dimer interface. Salt links were identified using a 4.0 Å interatomic cutoff and no angle cutoff. Hydrogen bonds were calculated using a distance cutoff of 4.0 Å and an angle cutoff of 90° (linear hydrogen bond has angle 0° in this convention). Hydrogen atoms were added to calculate hydrogen bonds but were omitted in all other calculations. In addition to distance and angle cutoffs, we used a *B*-factor cutoff, in which atoms with *B*-factors greater than 3σ above the mean were omitted from the analysis. Since the *B*-factor is a measure of the positional uncertainty, this cutoff provides a way to select the most meaningful salt links and hydrogen bonds. The 3σ *B*-cutoff for our model is 36.0 Å^2 and eliminates 33 atoms. This method was used in a previous analysis of the role of hydrogen bonds and salt links in thermostability (Tanner et al., 1996).

RESULTS

Subunit and Dimer Structure. The crystal structure of FRP is an isologous dimer of interlocking subunits. A topology diagram is in Figure 1, and a ribbon drawing of the dimer viewed down the 2-fold axis is in Figure 2. Overall, the two subunits are similar. The RMSD between the two subunits after least squares superposition of the main chain is 0.18 Å for main chain atoms and 0.36 Å for all atoms. The *B*-factors of the two subunits are also similar.

FIGURE 2: Stereoview of the FRP dimer viewed down the 2-fold axis with the two subunits colored yellow and red, FMN green, and PO_4 yellow. Black spheres are drawn at the CA atoms of the N- and C-termini. The N-termini are at the rear of the figure and are difficult to see. The C-termini are in the front of the figure near the ends of the K helices. The missing loops (residues 201−209) are represented by black bars connecting small spheres. Note that strand 3 is not labeled and that it runs nearly perpendicular to the plane of the page.

The *B*-factors refined to values consistent with a well-determined structure. The average *B*-factor is 19.5 Å^2 for all atoms, 13.8 Å^2 for FMN atoms, 23.1 Å^2 for water O1 atoms, and 32.9 Å^2 for atoms of phosphate ions. The largest *B*-factors (residue-averaged $B > 30$ Å^2) are found in the N-terminal residues of both chains, residues 23−24 of chain B and residues 185−188 of chain A. Residues 198−200 and residue 210 of both chains, which bracket the loop (201−209) that is unresolved in our structure, also have high *B*-factors. The highest atomic *B*-factor in the entire structure is 47.4 Å^2 (OH of Tyr A200).

Each subunit comprises two domains, a sandwich domain and an excursion domain. The first domain (residues 15−161, 226−240) is an $\alpha-\beta-\alpha$ sandwich consisting of a central four-stranded antiparallel β-sheet flanked by helices B and F on one side and by three helices (C, D, G) on the other side. Helices C, D, and G cover the main hydrophobic core of the subunit.

The second domain (residues 2−14, 162−225) is the excursion domain, and it consists of residues that reach out from one sandwich domain and embrace the other sandwich domain. The smaller part of the excursion domain is the N-terminal helix A, which contacts helices B and F of the other subunit (Figure 2). The larger part of the excursion domain (residues 162−225) begins with a 14-residue stretch of mostly unstructured polypeptide chain (residues 162−175) that connects strand 4 of one subunit to a short β-strand that runs parallel to strand 1 of the other subunit (see topology diagram). The chain then makes a reverse turn into helix I, followed by a flexible loop that is not resolved in our structure, and finally helix J. Helix J connects to the sandwich domain via residues 222−225. There are 316 hydrogen bonds within the A subunit and 319 in the B subunit. Each subunit also contains 8 salt links.

The interlocking nature of the dimer interface arises from the fact that the polypeptide chain starts in one half of the dimer, makes an excursion to the other half, and then returns to the first half of the dimer. This situation results in an unusually large, complementary dimer interface. The space-filling drawing of the dimer viewed down the 2-fold axis in Figure 3 shows the fit between the two subunits. The A_s buried in the dimer interface is 9352 Å^2. Hydrophobic residues contribute 51% of the interface area, while polar and charged residues contribute 31% and 18%, respectively. There are 57 intersubunit hydrogen bonds and 5 intersubunit salt links.

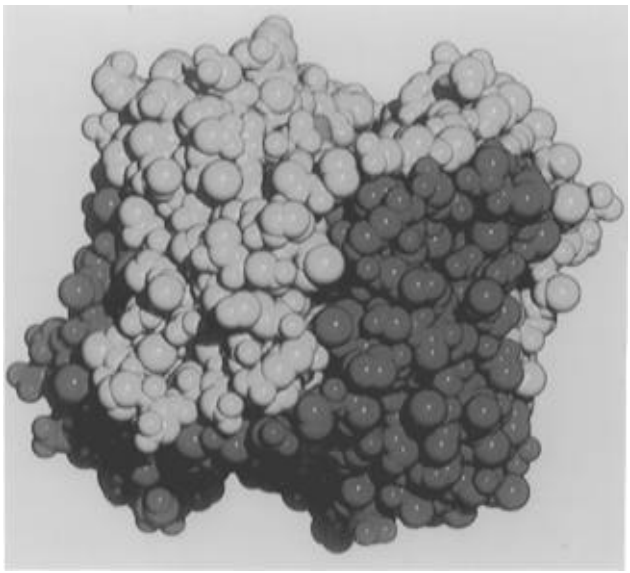

FIGURE 3: FRP dimer viewed down the 2-fold axis in an orientation identical to Figure 2. The two subunits are colored yellow and red, with the FMN in green.

There are two components to the dimer interface. The first component involves the packing of the excursion domains against the sandwich domains and accounts for 75% of the A_s buried in the interface. The second, smaller component of the dimer interface arises from the packing of the two sandwich domains and accounts for 25% of the A_s buried in the interface. This part of the dimer interface involves mainly the packing together of the long F helices. The interactions between these two helices are largely hydrophobic, with side chain−side chain hydrogen bonds between Gln A113 and Asn B114 being the only electrostatic interactions linking the F helices.

FMN Binding Site. Given the interlocking nature of the dimer, it is not surprising that the active site region is formed by elements from both subunits. FMN is bound in a crevice in the dimer interface with its isoalloxazine ring wedged between strand 3 of one subunit and a loop containing four contiguous Ser residues (38−41) from the other subunit

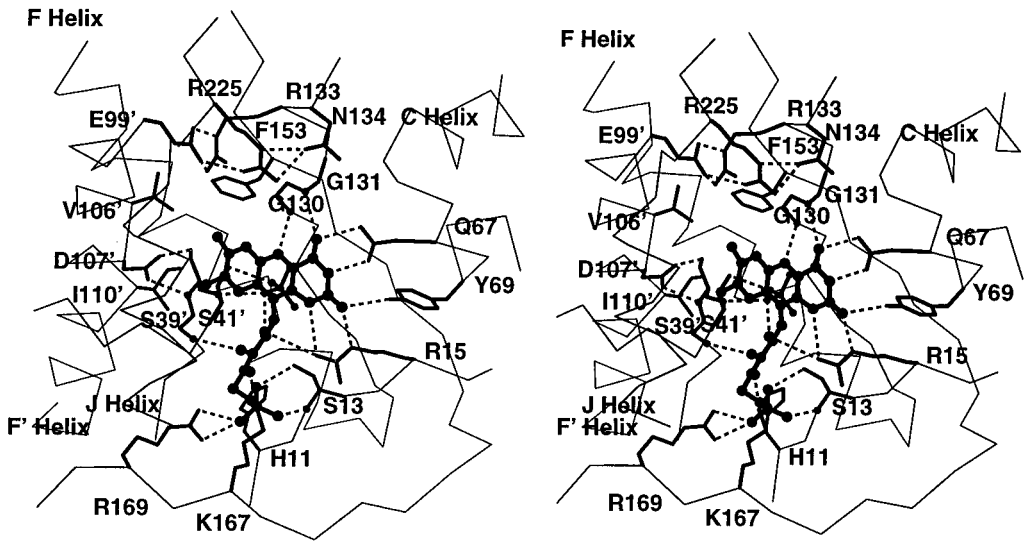

FIGURE 4: Stereoview of the FMN and its interactions with the protein. Hydrogen bonds are indicated by dashed lines. The molecular 2-fold axis, which bisects helices F and F′, is almost vertical. Residues marked with a prime are from the other subunit. Note the PO_4 anion hydrogen bonding to Ser 41′. Some residues are omitted for clarity.

(Figure 4). The plane of the isoalloxazine ring is perpendicular to the plane of the β-sheet. The dimethylbenzene edge of the isoalloxazine ring contacts the F helix from the other subunit.

Several electrostatic interactions stabilize the FMN (Figures 4 and 5). Excluding O5′, every N or O atom of the FMN that can form a hydrogen bond does indeed form one. The pyrimidine portion of the flavin hydrogen bonds to side chains of Arg 15, Tyr 69, and Gln 67 and to the main chain of Gly 130 and Gly 131. The latter two residues are part of a 3_{10} helix located directly above the flavin ring system. The ribityl chain is hydrogen bonded to Arg 15 and Lys 167 of one subunit and to Ser 39 of the other subunit. The flavin phosphate is anchored by hydrogen bonds to Arg 169, His 11, and Ser 13. While Ser 40 is close to the FMN, it does not hydrogen bond to FMN. Rather, it helps bury part of the *re* face of the benzenoid portion of the isoalloxazine ring while hydrogen bonding to Asp 107. Note that most of the hydrogen bonds between FMN and protein involve side chains.

In addition to the basic residues that hydrogen bond to FMN, Arg 225 and Arg 133 are significant for their location above the flavin. Electrostatics calculations performed using GRASP (Nicholls & Honig, 1992) show that the entire active site crevice except for the FMN phosphate is bathed in a positive potential field. This field probably steers substrates, which have phosphate moieties, to the active site. If the calculation is repeated with Arg 225 and Arg 133 uncharged, then the positive potential field is diminished and only covers the lower half of the active site.

Hydrophobic interactions are also present in the active site. The benzenoid portion of the isoalloxazine ring sits in a hydrophobic pocket formed by Phe 153 and Tyr 128 of one subunit and by Val 106 and Ile 110 of the other subunit.

The entire *si* face of the isoalloxazine ring is buried, as is the *re* face of the benzenoid portion of the isoalloxazine ring (Figure 6). Since the dimethyl edge of the isoalloxazine ring is buried, it is probably not involved in electron transfer, in contrast to what has been proposed for flavodoxins (Watenpaugh et al., 1973; Burnett et al., 1974). Catalysis likely occurs at the pyrimidine portion of the *re* face of the isoalloxazine ring.

The solvent accessibility of each atom of the flavin was determined using a 1.4 Å probe radius. Solvent and PO_4 ions were removed for this calculation. The values listed below are averages over the two subunits. The following FMN atoms, with A_s listed in parentheses, have significant ($A_s > 1$ Å^2) solvent exposure: OP2 (3.4), O4′ (2.6), O2′ (6.4), C2 (10.9), O2 (4.5), C4 (9.4), C4A (4.8), and C5A (1.1).

N1 and N5 are candidates for receiving the hydride from NADPH in the first step of catalysis. N1 is entirely buried ($A_s = 0.0$ Å^2) and N5 is almost completely buried ($A_s = 0.36$ Å^2). One might think that sequestration of N1 and N5 from solvent is inconsistent with their putative roles in catalysis. However, if the calculation is repeated with a smaller probe (radius 0.4 Å), we find that N5 exposes 1.6 Å^2 and N1 exposes 0.5 Å^2. This suggests that, neglecting conformational changes induced by substrate binding, N5 is the most likely candidate for hydride transfer.

The isoalloxazine ring is slightly bent, even though the flavin is fully oxidized. This feature is seen in other flavoenzymes. The conformation of the FMN ribityl chain differs from those found in other FMN-containing enzymes in the protein data bank. Curiously, the conformation of the FMN in FRP is similar to the FMN moiety of the FAD in butyryl-CoA dehydrogenase (Djordjevic et al., 1995). After their isoalloxazine rings were superimposed, the RMSD between the FMN of FRP and the FMN moiety of butyryl-CoA dehydrogenase is 0.7 Å for all atoms and 1.1 Å for the ribityl chain. In terms of sequence, overall protein fold, and function, there are no obvious similarities between the two enzymes.

We overlaid the FAD from butyryl-CoA dehydrogenase onto our structure so that its isoalloxazine ring was coincident with that of our FMN to gain insight as to why FRP does not use FAD as cofactor. The second phosphate of the pyrophosphate makes a steric clash with the guanidinium group of Arg 169, the ribose clashes with the side chain and main chain of Arg 169, and the adenine ring clashes with Pro 168. Repositioning of the adenine half of the FAD to avoid these steric overlaps produces other overlaps with Met 42, Tyr 192, and Met 196 in one direction and with helix A and helix B (opposite subunit) in the other direction. We

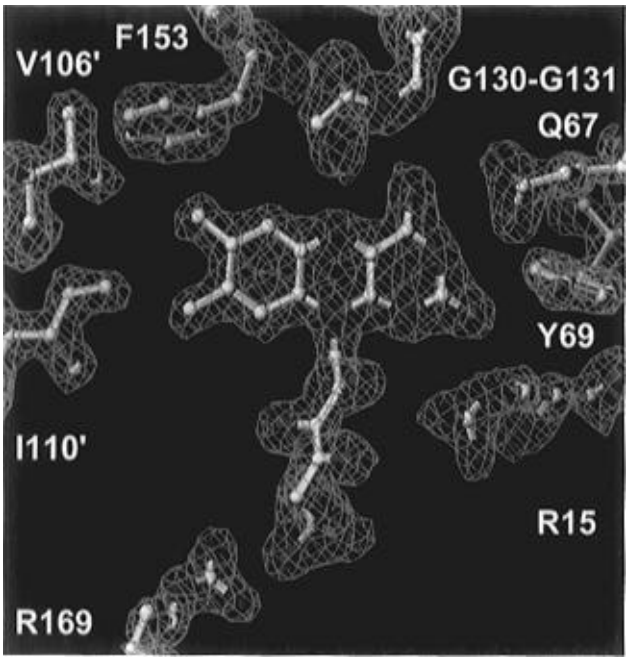

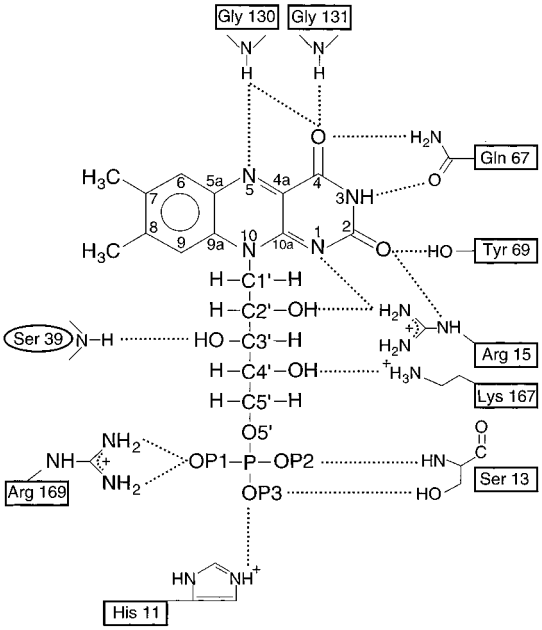

FIGURE 5: (a, top) FMN cofactor and some surrounding residues with $2F_o - F_c$ electron density contoured at 1.5σ. (b, bottom) Schematic diagram of FMN binding showing protein−FMN interactions. Note that Ser 39 (oval) is from the other subunit.

conclude that several steric interactions prevent FAD from binding as the cofactor.

Phosphate Site. The model contains one PO_4 anion per subunit that binds near the *re* face of the FMN on the pyrimidine end of the isoalloxazine ring (Figures 2 and 4). Phosphate oxygen atoms hydrogen bond to Ser 41 OG, Ser 41 N, and FMN O2′. In other enzymes, such as glyceraldehyde-3-phosphate dehydrogenase, inorganic phosphate sites are thought to represent the phosphate moieties of substrate (Kim et al., 1995). In our case, both FMN and NADPH have phosphate moieties.

DISCUSSION

Subunit and Dimer Structure. The crystal structure of FRP is a homodimer with an isologous 2-fold interaction. The

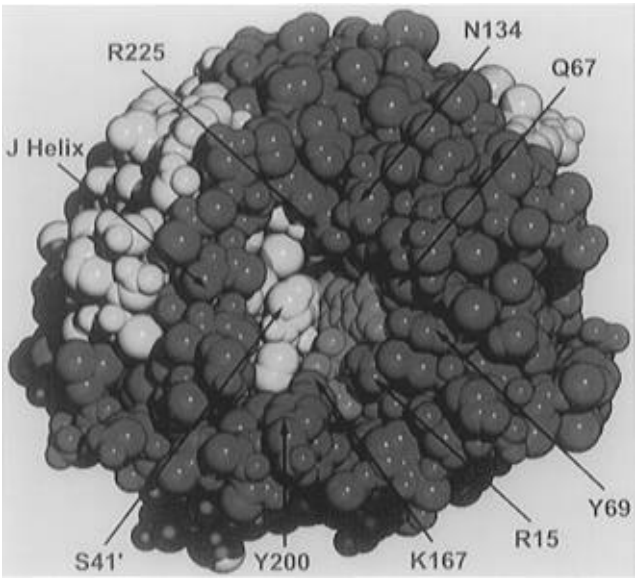

FIGURE 6: Active site crevice, with the two subunits colored yellow and red and FMN colored green. Water and phosphate are omitted for clarity. The orientation is that of Figure 4.

unique features of the FRP dimer are its large dimer interface and its interlocking subunits, rather than the type of interactions found in the interface. The dimer interface buries 9352 Å^2 of surface area, which is far more than one would expect for a protein of this molecular weight. The empirical estimate of $A_s = 0.006$MW (Jones & Thorton, 1995) predicts an interface area for FRP of about only 1600 Å^2, which suggests that the FRP dimer is not like other known dimers. The percentage A_s buried per subunit is 37%, which exceeds that of all the dimers surveyed in a recent review article on dimer interfaces (Jones & Thorton, 1995). For comparison, the highest value of A_s buried per subunit in the survey is 29% for trp repressor.

The 57 intersubunit hydrogen bonds observed in FRP are within the error limits of the empirical estimate of 0.88 (±0.4) hydrogen bonds per 100 Å^2 of interface surface area (Jones & Thorton, 1995). Likewise, the composition of the interface in terms of hydrophobic, polar, and charged residues is similar to other dimers.

There are other cases of dimers formed by interpenetrating subunits. Examples include the helical cytokines interleukin-10 (Walter & Nagabhushan, 1995; Zdanov et al., 1995) and interferon-γ (Ealick et al., 1991; Samudzi & Rubin, 1993). In these proteins, two helices of one subunit intertwine with the other subunit. The FRP dimer is different from interleukin-10 and interferon-γ in that the degree of interpenetration of the two subunits is much greater in FRP and the interface involves sheet as well as helical secondary structure.

Comparison to Other Flavoenzymes. We compared the structure of FRP to other flavin-containing proteins to see if it belongs to a known structural class of flavoenzyme. A total of 39 flavoproteins were extracted from the protein data bank. Most of them can be classified into one of four structural families. Examples of these families are flavodoxin, glycolate oxidase, glutathione reductase, and ferredoxin $NADP^+$ reductase.

Flavodoxins bind FMN at the carboxyl ends of a five-stranded parallel β-sheet with the dimethylbenzene edge of the FMN exposed to solvent (Watenpaugh et al., 1973; Burnett et al., 1974; Smith et al., 1983; Fukuyama et al.,

1990; Rao et al., 1992). The glycolate oxidase family uses an eight-stranded parallel β-barrel to bind FMN (Lindqvist, 1989). The glutathione reductase-like enzymes use a Rossmann-type fold to bind the ADP portion of FAD (Karplus & Schulz, 1987). In the $NADP^+$ reductase family, the flavin binding domain is a six-stranded antiparallel β-barrel core with a Greek key motif (Karplus et al., 1991). This class includes both FMN and FAD-containing enzymes. Other flavoproteins that do not fall into these four categories include the *lux*F protein (Moore et al., 1993) and acyl- and butyryl-CoA dehydrogenase (Kim et al., 1993; Djordjevic et al., 1995). Each *lux*F monomer consists of a seven-stranded parallel β-barrel and seven α-helices, and there are myristylated FMN molecules bound at the dimer interface and at the chain termini. The FAD in acyl- and butyryl-CoA dehydrogenase binds in a crevice formed by two helical domains on one side and by a β-sheet domain on the other side. FRP does not resemble any of these enzymes in terms of overall fold, dimeric structure, or FMN binding motif.

There is, however, one intriguing similarity between FRP and other flavoenzymes. All but one of the flavoproteins surveyed have a hydrogen bond between flavin N3 and a proton acceptor in the protein. The only exception is flavocytochrome *c* sulfide dehydrogenase (Chen et al., 1994), which is a member of the glutathione reductase structural family. In FRP the proton acceptor is Gln 67 OE1, while it is a main chain carbonyl oxygen in about one-half of the enzymes studied. The fact that this protein−flavin interaction is conserved in many flavoenzymes that have different overall structures and functions suggests that it is an important component of flavin binding and catalysis.

The FRP class of flavoenzyme appears to include NOX from *T. thermophilus*, whose crystal structure was solved recently (Hecht et al., 1995). Since the structure of NOX was not available at the time this manuscript was prepared, we were not able to perform a detailed comparison. The two structures seem to be similar enough to be classified in the same structural family, but there are also some important differences, which we now describe.

FRP and NOX share 30% sequence identity, but FRP has 35 more residues than NOX. This leads to two main structural differences. First, NOX has an extra 16-residue flexible helix inserted between helices E and F of our topology diagram. Second, the C-terminus of NOX is effectively at residue 179 of FRP. NOX therefore lacks helices I, J, and K of FRP, although helix J of FRP could be structurally equivalent to the 16-residue flexible helix of NOX. Because the final element of secondary structure in NOX is the short fifth strand at residues 176−178 (FRP numbering), the NOX dimer does not display the same degree of interlocking that we see in FRP. Finally, the PO_4 binding site was not identified in NOX.

Catalytic Mechanism. The first step in catalysis is the reduction of FMN by NADPH, which involves hydride transfer from NADPH C4 to either N1 or N5 of the flavin cofactor. Since the *si* face of the FMN is completely buried, hydride transfer occurs at the *re* face. We determined the accessibility of N1 and N5 to probes with radii 1.4 Å (approximating solvent) and 0.4 Å (approximating hydride). N5 is sequestered from solvent but is accessible to the small probe. N1 is sequestered from both probes. Therefore, we predict that hydride transfer from NADPH to FMN occurs through N5.

Kinetics studies are consistent with a ping-pong bisubstrate−biproduct reaction mechanism in which the second step of catalysis is the reduction and release of exogenous FMN substrate. This scenario is consistent with our structure on three accounts. First, the FMN cofactor is bound tightly by 16 hydrogen bonds. Every N or O atom of the oxidized FMN that is capable of making a hydrogen bond to the enzyme does form one, excluding O5′. Second, the FMN binding pocket is a narrow crevice that could not accommodate a ternary complex of FMN cofactor, NADPH, and FMN substrate. Thus, $NADP^+$ product would have to be released before FMN substrate could bind. Third, the average *B*-factor for FMN atoms is only 13.8 $Å^2$, compared to 19.5 $Å^2$ for the protein, indicating again that the cofactor is bound tightly.

From biochemical studies it is known that FRP has less affinity for its FMN cofactor after it is reduced. This can also be rationalized in terms of our structure. Upon reduction of the flavin, presumably the flavin N5 atom is protonated and the hydrogen bond between flavin N5 and Gly 130 N could be weakened or lost. Thus, the apoenzyme's affinity for reduced FMN cofactor is less than that for oxidized FMN. However, there would still be as many as 15 hydrogen bonds available to stabilize the reduced FMN cofactor. If the reduced FMN cofactor remains bound by the enzyme, it cannot participate as a substrate in a sequential mechanism, leaving the ping-pong mechanism described above.

FMN and NADPH Specificities. FRP specifically uses FMN as cofactor and NADPH as substrate rather than FAD and NADH. The structure of butyryl-CoA dehydrogenase, which binds FAD in the same conformation as the FMN in FRP, provides clues as to why FRP does not use FAD. If FRP were to bind FAD in the conformation observed in butyryl-CoA dehydrogenase, then several close contacts between FAD and FRP would result, particularly in the area of residues 167−169.

We conclude that FRP uses several hydrogen bonds and a hydrophobic pocket to recognize and bind FMN, and it rejects FAD as a cofactor on the basis of steric overlap. Since the main steric hindrance to FAD binding comes from both the main chain and side chains of residues 167−169, it would be difficult to devise single site mutations that would alter FMN specificity.

Currently, we do not have direct structural evidence of how FRP binds NADPH. Native crystals soaked in 1−10 mM $NADP^+$ deteriorate and are unusable. Crystals soaked in 50−100 mM $NADP^+$ appear to be stable when viewed through a light microscope; however, they turn from yellow to clear and fail to diffract X-rays. Ongoing soaking and cocrystallization studies should shed some light on this aspect of the catalytic mechanism.

One speculation is that the flexible loop (residues 201−209) is involved in NADPH binding. This loop is not resolved in our structure, but NADPH is long enough to span from the *re* face of the FMN to the region we expect to find residues 201−209. This loop contains two residues, Arg 203 and Lys 208, that potentially could bind the phosphate moiety of the adenosine and explain why FRP is NADPH specific.

We pursued this hypothesis by aligning the sequence of FRP with those of FRD (Izumoto et al., 1994) and NOX because the latter two enzymes are NADH specific. FRP and FRD have only 16% sequence identity and probably have

different structures; therefore, the alignment was not helpful. FRP and NOX share 30% sequence identity and have similar structures. The major structural difference is that FRP has extra elements of secondary structure, including the 201−209 loop. This supports the notion that this loop might be responsible for the NADPH specificity of FRP.

Significance of the Inorganic PO_4 Site. A PO_4 is bound near the pyrimidine portion of the *re* face of the isoalloxazine ring, which is where hydride transfer from NADPH is expected to occur. Therefore, one of the phosphate oxygen atoms could represent the nicotinamide carbonyl oxygen. If so, it indicates that Ser 41 is important for binding NADPH because Ser 41 hydrogen bonds to the PO_4 in our crystal structure.

Another possibility is that the PO_4 site is involved in the first step in binding oxidized FMN substrate or NADPH or both. With regard to flavin substrate binding, the PO_4 site could be involved but appears not to be critical on the basis that riboflavin is an effective substrate (M. Liu, B. Lei, and S.-C. Tu, unpublished results).

Whereas it is unlikely that the PO_4 we observe represents the actual adenosine 2′-phosphate or 5′-pyrophosphate of NADPH, it could be a structural motif that coordinates the binding of the NADPH. A phosphate moiety of NADPH could be attracted to this PO_4 site for its initial landing. Once bound, a subsequent repositioning of NADPH could take place to locate its final binding orientation.

Role of FRP in Bacterial Bioluminescence. Unlike most flavoenzymes, bacterial luciferase uses $FMNH_2$ as a substrate rather than a tightly bound cofactor (Baldwin & Ziegler, 1992; Tu & Mager, 1995). Since flavin reductases generate reduced FMN and they are present in luminous bacteria, they could be an important source of $FMNH_2$ for luciferase. This idea is supported by the fact that light can be generated in vitro by luciferase when the sole source of $FMNH_2$ is flavin reductase catalysis. The dynamics of the transfer of $FMNH_2$ between the active sites of the two enzymes, however, is not known.

One scenario is that, in vivo, flavin reductases contribute to the pool of free $FMNH_2$ from which luciferase draws its substrate. Recent in vitro kinetics experiments on *V. harveyi* FRP, however, now suggest an additional role for this enzyme. The catalytic mechanism of FRP shifts from ping-pong bisubstrate−biproduct in the absence of luciferase to a sequential mechanism when the kinetics of FRP are followed in the presence of luciferase by measuring light emission. This shift implies the formation of a ternary complex containing enzyme, FMN substrate, and NADPH in the coupled assay (Lei & Tu, 1994).

From the structure, however, we know that the binding cleft will not accommodate simultaneously the FMN cofactor, an FMN substrate, and NADPH. Therefore, the only explanation is that the FMN cofactor can serve also as a substrate in the presence of luciferase in vitro. Since both oxidized and reduced FMN cofactor are bound tightly by FRP, it is difficult to explain how FRP can lose its $FMNH_2$ cofactor to luciferase unless the two enzymes form a specific complex that weakens cofactor binding.

This complex might feature interactions between luciferase and FRP side chains that hydrogen bond to the FMN cofactor since most of the hydrogen bonds that stabilize the FMN cofactor in FRP involve side chains. These interactions could alter the free energy of binding such that the affinity of FRP for reduced FMN cofactor is significantly lower than that for oxidized cofactor. This hypothesis could be tested by mutagenesis of FRP residues that hydrogen bond to FMN. Mutants that shift reaction kinetics from ping-pong to sequential in the absence of luciferase and significantly diminish light production in the coupled assay might be the residues that interact with luciferase. With the structures of FRP and luciferase (Fisher et al., 1995) we now have a rational basis for designing such mutation experiments and for modeling the interactions between these two enzymes.

ACKNOWLEDGMENT

We thank George Phillips for the use of the R-axis detector at Rice University.

REFERENCES

Baldwin, T. O., & Ziegler, M. M. (1992) in *Chemistry and Biochemistry of Flavoenzymes* (Müller, F., Ed.) CRC Press, pp 467−530, Boca Raton, FL.

Brünger, A. T. (1992) *X-PLOR version 3.1. A system for x-ray crystallography and NMR*, Yale University Press, New Haven.

Burnett, R. M., Darling, G. D., Kendall, G. S., LeQuesne, M. E., Mayhew, S. G., Smith, W. W., & Ludwid, M. L. (1974) *J. Biol. Chem. 249*, 4383−4392.

Chen, Z.-w., Koh, M., Driessche, G. v., Beeumen, J. J. v., Bartsch, R. G., Meyer, T. E., Cusanovich, M. A., & Mathews, F. S. (1994) *Science 266*, 430−432.

Chikuba, K., Yubisui, T., Shirabe, K., & Takeshita, M. (1994) *Biochem. Biophys. Res. Commun. 198*, 1170−1176.

Covès, J., & Fontecave, M. (1993) *Eur. J. Biochem. 211*, 635−641.

Covès, J., Nivière, V., Eschenbrenner, M., & Fontecave, M. (1993) *J. Biol. Chem. 268*, 18604−18609.

Djordjevic, S., Pace, C. P., Stankovich, M. T., & Kim, J.-J. P. (1995) *Biochemistry 34*, 2163−2171.

Ealick, S. E., Cook, W. J., Vijay-Kumar, S., Carson, M., Nagabhushan, T. L., Trotta, P. P., & Bugg, C. E. (1991) *Science 252*, 698−702.

Engh, R. A., & Huber, R. (1991) *Acta Crystallogr. A47*, 392−400.

Fisher, A. J., Raushel, F. M., Baldwin, T. O., & Rayment, I. (1995) *Biochemistry 34*, 6581−6586.

Fontecave, M., Eliasson, R., & Reichard, P. (1987) *J. Biol. Chem. 262*, 12325−12331.

Fukuyama, K., Wakabayashi, S., Matsubara, H., & Rogers, L. J. (1990) *J. Biol. Chem. 265*, 15804−15812.

Furey, W., & Swaminathan, S. (1996) in *Macromolecular Crystallography, A Volume of Methods in Enzymology* (Carter, C., & Sweet, R., Eds.) Academic Press, Orlando, FL.

Gaudu, P., Touati, D., Nivière, V., & Fontecave, M. (1994) *J. Biol. Chem. 269*, 8182−8188.

Gerlo, E., & Charlier, J. (1975) *Eur. J. Biochem. 57*, 461−467.

Hallé, F., & Meyer, J. (1992) *Eur. J. Biochem. 209*, 621−627.

Hasan, N., & Nestor, E. W. (1978) *J. Biol. Chem. 253*, 4987−4992.

Hecht, H. J., Erdmann, H., Park, H. J., Sprinzl, M., & Schmid, R. D. (1995) *Nat. Struct. Biol. 2*, 1109−1114.

Higashi, T. (1990) *PROCESS: A program for indexing and processing R-AXIS II imaging plate data*, Rigaku Corp., Tokyo.

Inouye, S. (1994) *FEBS Lett. 347*, 163−168.

Izumoto, Y., Mori, T., & Yamamoto, T. (1994) *Biochim. Biophys. Acta 1185*, 243−246.

Jablonski, E., & DeLuca, M. (1978) *Biochemistry 17*, 672−678.

Jones, S., & Thorton, J. M. (1995) *Prog. Biophys. Mol. Biol. 63*, 31−65.

Jones, T. A. (1978) *J. Appl. Cryst. 11*, 268−272.

Jones, T. A., Zou, J.-Y., Cowan, S. W., & Kjeldgaard, M. (1991) *Acta Crystallogr. A47*, 110−119.

Kabsch, W. (1988) *J. Appl. Crystallogr. 21*, 916−924.

Karplus, P. A., & Schulz, G. E. (1987) *J. Mol. Biol. 195*, 701−729.

Karplus, P. A., Daniels, M. J., & Herriott, J. R. (1991) *Science 251*, 60−66.

Kim, H., Feil, I. K., Verlinde, C. L. M. J., Petra, P. H., & Hol, W. G. J. (1995) *Biochemistry 34*, 14975−14986.
Kim, J.-J. P., Wang, M., & Paschke, R. (1993) *Proc. Natl. Acad. Sci. U.S.A. 90*, 7523−7527.
Laskowski, R. A., MacArthur, M. W., Moss, D. S., & Thornton, J. M. (1993) *J. Appl. Crystallogr. 26*, 283−291.
Lei, B., & Tu, S.-C., Eds. (1994) *Characterization of the Vibrio harveyi FMN:NADPH oxidoreductase expressed in Escherichia coli*. *Flavins and Flavoproteins*, Walter de Gruyter, Berlin.
Lei, B., Liu, M., Huang, S., & Tu, S.-C. (1994) *J. Bacteriol. 176*, 3552−3558.
Lindqvist, Y. (1989) *J. Mol. Biol. 209*, 151−166.
Luzzati, P. V. (1952) *Acta Crystallogr. 5*, 802−810.
Messerschmidt, A., & Pflugrath, J. W. (1987) *J. Appl. Crystallogr. 20*, 306−315.
Michaliszyn, G. A., Wing, S. S., & Meighen, E. A. (1977) *J. Biol. Chem. 252*, 7495−7499.
Moore, S. A., James, M. N. G., O'Kane, D. J., & Lee, J. (1993) *EMBO J. 12*, 1767−1774.
Nicholls, A., & Honig, B. (1992) *GRASP: graphical representation and analysis of surface properties*, Columbia University, New York.
Quandt, K. S., Xu, F., Chen, P., & Hultquist, D. E. (1991) *Biochem. Biophys. Res. Commun. 178*, 315−321.
Rao, S. T., Shaffie, F., Yu, C., Satyshur, K. A., Stockman, B. J., Markley, J. L., & Sundaralingam, M. (1992) *Protein Sci. 1*, 1413−1427.
Samudzi, C. T., & Rubin, J. R. (1993) *Acta Crystallogr. D49*, 513−521.
Smith, W. W., Pattridge, K. A., Ludwig, M. L., Petsko, G. A., Tsernoglou, D., Tanaka, M., & Yasunobu, K. T. (1983) *J. Mol. Biol. 165*, 737−755.
Tanner, J., & Krause, K. L. (1994) *Rigaku J. 11*, 4−10.
Tanner, J., Lei, B., Liu, M., Tu, S.-C., & Krause, K. L. (1994) *J. Mol. Biol. 241*, 183−187.
Tanner, J. J., Hecht, R. M., & Krause, K. L. (1996) *Biochemistry 35*, 2597−2609.
Tu, S.-C., & Mager, H. I. X. (1995) *Photochem. Photobiol. 62*, 615−624.
Tu, S.-C., Becvar, J. E., & Hastings, J. W. (1979) *Arch. Biochem. Biophys. 193*, 110−116.
Walter, M. R., & Nagabhushan, T. L. (1995) *Biochemistry 34*, 12118−12125.
Watanabe, H., & Hastings, J. W. (1982) *Mol. Cell. Biochem. 44*, 181−187.
Watenpaugh, K. D., Sieker, L. C., & Jensen, L. H. (1973) *Proc. Natl. Acad. Sci. U.S.A. 70*, 3857−3860.
Zdanov, A., Schalk-Hihi, C., Gustchina, A., Tsang, M., Weatherbee, J., & Wlodawer, A. (1995) *Structure 3*, 591−601.
Zenno, S., & Saigo, K. (1994) *J. Bacteriol. 176*, 3544−3551.
Zhang, K. Y. J., & Main, P. (1990) *Acta Cystallogr. A46*, 377−381.

BI961400V